كلية الهندسة

Journal of Engineering Sciences Assiut University Faculty of Engineering

Vol. 48, No. 5

September 2020

PP. 805-829

جامعة أسيوط

A NUMERICAL STUDY ON SEISMIC PERFORMANCE EVALUATION OF RC RECTANGULAR COLUMNS STRENGTHENED WITH CFRP SHEETS

Mena Gamel Youssef[*1], Abdel-Rahman M. Ahmed [2], Mohamed M. Ahmed[2], Omar A. Farghal[2]

[1]M.Sc. graduate Student, Civil Engineering Department, Faculty of Engineering, Assiut University, Egypt. [*]menagamel2018@gmail.com

[2]Civil Engineering Department, Faculty of Engineering, Assiut University, Egypt

Received 21 July 2020; Revised 9 September 2020; Accepted 15 September 2020

ABSTRACT

External confinement of reinforced concrete columns using fiber-reinforced polymer (FRP) sheets can significantly enhance their seismic behavior. This research presents a numerical investigation to evaluate the seismic performance of RC rectangular columns with limited cross-sections' aspect ratios (1, 1.5, and 2) strengthened with a fully wrapped CFRP jacket under constant axial and pushover lateral loads. Therefore, a three-dimensional finite element model was implemented via ABAQUS software, which has been adopted in this study, where the proposed model showed a reliable agreement with the previous experimental work. The studied parameters are longitudinal steel reinforcement ratio, CFRP confinement ratio, and axial load/capacity ratio for each cross-section aspect ratio. The obtained numerical results have proved that the external wrapping of RC rectangular columns with CFRP sheets has effectively increased drift capacity ratios for cross-sections aspect ratios 1, 1.5, and 2. Moreover, the strengthening of RC rectangular columns using external CFRP wrapping increases the nominal shear and flexural strengths of the strengthened columns. Also, the effect of increasing the longitudinal steel reinforcement ratio can significantly decrease the ultimate lateral displacement and drift capacity ratios. Besides, with the increase of the axial load/capacity ratios, the

drift capacity ratios significantly decrease for the strengthened RC rectangular columns.

KEYWORDS: Strengthened RC Columns; CFRP; Seismic Behavior; Ductility; flexural strength.

1. Introduction

Reinforced concrete (RC) columns, which have been designed to obsolete codes, are usually do not have adequate transverse reinforcement, which leads to brittle shear failure [1-3]. So, the need to retrofit and strengthen these seismically deficient columns is essential to enhance their seismic performance. The traditional strengthening techniques, such as: concrete jacketing [4] and steel jacketing [5-7] improve both: strength and stiffness for the strengthened RC columns. However, these techniques have several problems, such as: architecture space reduction, long time for execution, and corrosion of the steel jacket. FRP composites have been widely used in recent decades to strengthen and retrofit RC columns. The success of FRP strengthening techniques has attributed to many advantages of FRP materials, such as: high strength-to-weight ratio, excellent corrosion resistance, high durability, great ductility, and fast installation in the field [8]. Furthermore, FRP strengthening does not increase the stiffness of the structure, hence no change in the structural dynamic response [9]. Several experimental and numerical studies have discussed the behavior of FRP-confined rectangular RC columns under axial loading, [10, 11], these studies have demonstrated that FRP confinement considerably enhances the strength and ductility of the strengthened RC columns. Regarding the RC columns exposed to earthquake load, the FRP confinement significantly improves their ductility and the dissipation energy capacity [12]. Moreover, it prevents brittle shear failure and allows formation of a plastic hinge mechanism [13]. Furthermore, the FRP external wrapping of RC columns can decrease crack width, which limits the apparition of the damage [14], as well as, it can delay the longitudinal reinforcement buckling and accordingly prevent the crushing of concrete cover [15, 16]. Besides, from the literature, using CFRP anchor dowels with CFRP external wrapping in strengthening RC columns increases the ultimate drift ratio by more than two times of RC columns with no strengthening [17]. Moreover, it has demonstrated that retrofitting of RC columns with CFRP sheets can effectively prevent the failure in the lap splice region [18]. Finally, the confinement of RC columns with FRP composites

can significantly increase the shear strength of these columns, which leads to more safety against sudden failure [19, 20]. After all, this research presents an attempt to understand and evaluate numerically the seismic performance of the interior RC rectangular columns strengthened with CFRP wrapping having cross-sections aspect ratios of (1, 1.5, and 2) in the moderate importance buildings.

2. Finite Element Modeling

The used finite element software in this study is ABAQUS [21], in which it enables the construction of models considering geometrical and material nonlinearity. The constructed finite element model consists of five parts: the concrete column, loading stub, footing, steel reinforcement, and CFRP jacket. The concrete column, loading stub, and footing were created as 3D solid parts. Then, the longitudinal and transverse steel reinforcement are modeled as 3D wire parts, while the CFRP sheets are created as 3D shell parts, as shown in **Figure 1**.

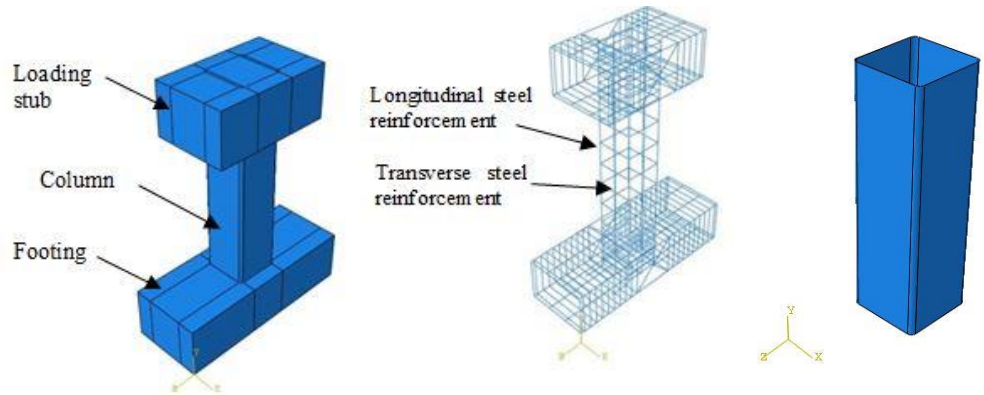

(a) Concrete parts (b) Steel reinforcement cage (c) CFRP jacket

Figure 1 Description of concrete (C3D8R elements), steel reinforcement (T3D2 elements), and CFRP jacket (S4R element) parts assembled in the finite element model

2.1. Materials modeling

2.1.1. Concrete modeling

The used concrete material has a cylindrical compressive strength (f_c') equals to 29.6 MPa and an elastic modulus of 29000 MPa, according to the test results reported by Ouyang, et al. (2017) [20]. The definition of concrete

material in ABAQUS consists of two main parts: elastic and plastic behaviors. The elastic behavior has defined by the elastic modulus and poison's ratio (υ_c), which is assumed in this study to be 0.2. The concrete damage plasticity model (CDPM) is used to capture concrete plastic behavior and stiffness degradation in both tension and compression. In addition, the default plasticity parameter values recommended by ABAQUS [21] used for modeling the unconfined concrete, as shown in **Table 1**. For FRP-confined concrete, the ratio of biaxial compressive yield stress to the uniaxial compressive strength (f_{b0}/f_{c0}) parameter is defined by Papanikolaou, et al. **(2007**) [22], as indicated in **Figure 2-a,** which is given by the following equation:

$$f_{b0}/f_{c0} = 1.5(f_c')^{-0.075} \quad (1)$$

Equation (1) is used by Hany, et al. (2016) [23] and Tao, et al. (2013) [24] to simulate the FRP-confined concrete in their finite element analysis so, it is used in this study. Also, the slope of the concrete compression meridian has presented using the dilation angle parameter (Ψ), which is assumed to be 30^o, as reported by Yuan, F., et al. (2017) [25].

Table 1 Plasticity parameters for unconfined concrete

Parameter name	Assigned value
Dilation angle (Ψ)	30^o
Eccentricity parameter (ϵ)	0.1
The ratio of biaxial compressive yield stress to the uniaxial compressive yield stress (f_{b0}/f_{c0})	1.16
The ratio of the second stress invariant on the tensile meridian to that on the compression meridian (k_c)	0.67
Viscosity parameter (μ)	0.005

Regarding the ratio of the second stress invariant on the tensile meridian to that on the compression meridian k_c parameter, as indicated in **Figure 2-b,** the proposed equation by **Ozbakkaloglu, et al. (2016)** [26] was adopted in this study, which is given by the following equation:

$$k_c = 0.71(f_c')^{-0.025} \quad (2)$$

Where, f_c' is the unconfined concrete compressive strength.

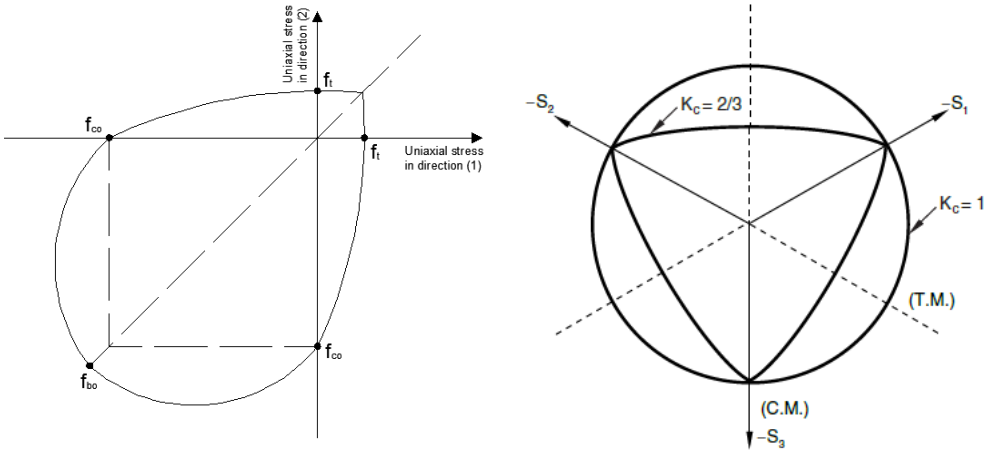

(a) Biaxial failure surface of concrete

(b) Yield surfaces in the deviator plane, corresponding to different values of k_c

Figure 1 Definition of plasticity parameters used in the finite element model

The definition of the dilation angle Ψ has a significant effect on the lateral confinement pressure and the strength of FRP-confined concrete. Hany, et al. (2016) [23] equation is used in the presented study to evaluate the dilation angle value Ψ as a function of unconfined concrete compressive strength f_c' and the radial stiffness of FRP jacket k_l, which is given by the following:

$$\Psi = -1.4587\frac{k_l}{f_c'} + 57.296\,, with\ k_l = \frac{2E_{frp}nt_{frp}}{D} \text{ for } 0 < \frac{k_l}{f_c'} \leq 40 \qquad (3)$$

Where, E_{frp} is the elastic modulus of FRP in the fiber direction, n is the number of FRP plies, t_{frp} is the thickness of the FRP ply, and D is the equivalent diameter of the column cross-section. The stress-strain relation proposed by Saenz, L.P. (1964) [27] is adopted in the presented study to simulate the unconfined concrete such as: control specimens, loading stub, and footing. Regarding FRP-confined concrete modeling, the proposed model by Ferrotto, M., et al. (2018) [28] is adopted due to its simplicity and acceptable accuracy. Ferrotto, M., et al. (2018) [28] proposed this model based on a modification of the stress-strain relationship proposed by Popovics, S. (1973) [29]. The stress-strain model is considered to consist of three branches. The first branch is ascending to the unconfined concrete strength/strain (f_{co}, ε_{co}). Then, the strain increases from (ε_{co}) to a transition strain value (ε_c^*) at a constant strength (f_{co}), which named the second branch

followed by the softening behavior (third branch) Popovics, S. (1973) [29], with changing the unconfined strain value (ε_{co}) by a transfer strain value (ε_c^*), and the slope of the softening branch was modified as shown in **Figure 3-a**. Regarding the concrete in tension, it follows as a linear elastic behavior until reaching the tensile strength value $\mathfrak{s}_{t0}$, which is assumed to equal 0.1 f_c' in current study. Then, a linear decrease in the stress was followed, which is defined as a tension stiffening behavior. A simplified model is adopted, as reported by Wahalathantri, B.L., et al. (2011) [30], which simulated the tension stiffening, as illustrated in **Figure 3-b**.

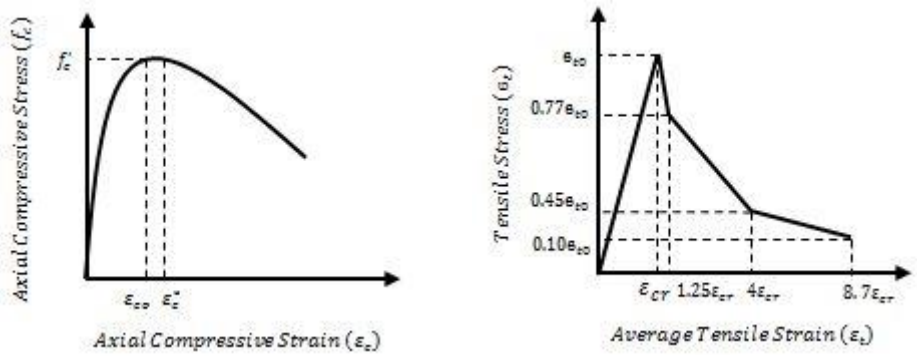

(a) FRP-confined concrete stress-strain model

(b) Concrete tension stiffening stress-strain model

Figure 2 Numerical models for concrete adopted in finite element model

2.1.2. Steel reinforcement modeling

The elastic-perfectly plastic stress-strain model is used as a numerical model for steel reinforcement, as recommended by Taghia, P. and S.A. Bakar (2013) [31] and Hajsadeghi, et al. (2011) [32]. Table 2 shows the used mechanical properties of the steel reinforcement, as reported by Ouyang, et al. (2017) [20]. Moreover, the poison's ratio is assumed as 0.3 for both transverse and longitudinal steel reinforcement materials.

2.1.3. CFRP modeling

The used CFRP material is unidirectional, and the modulus of elasticity in fiber direction has great importance, which is the fiber in a perpendicular direction to the column's longitudinal axis. Therefore, the CFRP material is modeled in ABAQUS as a linear elastic material. **Table 3** shows the mechanical properties of the used CFRP sheet, measured from flat coupon test, as reported in Ouyang, et al. (2017) [20], and the used poison's ratio assumed as 0.3.

Table 2 Mechanical properties of steel reinforcement

Reinforcement type	Diameter (mm)	Yield strength, f_{sy} (MPa)	Ultimate strength, f_{su} (MPa)	Elastic modulus, E_s (GPa)
Transverse steel	6	315	530	200
Longitudinal steel	16	386	587	205
	18			
	20			

Table 3 Mechanical properties of CFRP material

FRP type	Nominal thickness, t_{frp} (mm/ply)	Tensile strength, f_{frpu} (MPa)	Elastic modulus, E_{frp} (GPa)	Ultimate tensile strain, ε_{frpu} (%)
CFRP	0.167	3110	213	1.47

2.2 Boundary conditions and constrains between parts

The base of the column was restrained against movement and rotation in X, Y, and Z directions to simulate the experimental test condition. The contact between steel reinforcement and concrete elements simulated by the embedded constraint option. In addition, the contact between the FRP jacket and concrete column is modeled using the tie constraint option.

2.3 Loading procedure and mesh generation strategy

The applied loads are: constant axial load, then pushover lateral loading, besides the obtained results verified by the envelope experimental hysteresis loops (average backbone curves from the push and pull directions), as reported by Ouyang, et al. (2017) [20]. The concrete column, loading stub, and footing were modeled as C3D8R element, i.e., a solid element linear brick with eight nodes and three-dimensional stress element with reduced integration. Also, the element used for the CFRP jacket was S4R, i.e., a shell element with four nodes reduced integration and a finite membrane strain element. Regarding steel reinforcement, the used element was T3D2, i.e., truss element, linear three dimensional with two nodes element. The density of the mesh is specified through seeding the edges of the model assembly, to choose the optimum seeding size, a convergence study has been done on a square column wrapped with two CFRP layers named C-C2 reported in Ouyang, et al. (2017) [20]. The convergence study results showed that there is no difference in results in the case of seeding size less than 40mm, as shown in **Figure 4-a**. From the obtained convergence results, the seeding was

applied uniformly with an approximately global size of 40mm, **Figure 4-b** shows the three-dimensional model for the adopted meshing.

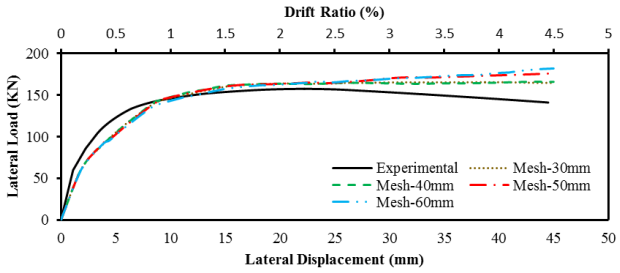

(a) Effect of seeding elements size on the convergence

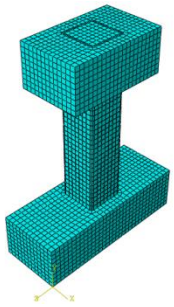

(b) 3Ds model for meshing

Figure 4 Mesh convergence study results

2.4 Verification of numerical model against experimental work

To verify the accuracy of the finite element model, the experimental work by Ouyang, et al. (2017) [20], is considered for comparison. Ouyang et al. has tested experimentally six columns with dimensions of 300×300×1000 mm: where, one control column, and five FRP-retrofitted columns under constant axial and lateral cyclic loads. The control column (C0) and CFRP-retrofitted column with two layers (C-C2) were chosen in this verification where, the details of these columns are indicated in **Table 4**. The failure criteria of the tested columns were following the same criteria used in experimental reference by Ouyang, et al. (2017) [20]. Where, the control column (C0) was characterized by diagonal shear wide cracks, followed by longitudinal reinforcement buckling, as shown in **Figure 5**. For the CFRP-confined column (C-C2) the endpoint of lateral-load displacement was determined at which CFRP-wraps rupture, when it was reached to ultimate stress, also at this point it can be observed visible horizontal cracks concentrated at the critical regions, as indicated in **Figure 6**. Also, **Figure 7** shows the results of the load-displacement relationships, which are in a reliable agreement with experimental work.

Table 4 Properties of selected specimens for verification, Ouyang, et al. **(2017)** [20]

Specimen code	f_c' (MPa)	Longitudinal steel reinforcement	Transverse steel reinforcement	CFRP jacket
C0	29.6	8 bars, 18 mm diameter	Stirrup 6 mm diameter, spaced at	----------
C-C2	29.6	8 bars, 18 mm diameter	Stirrup 6 mm diameter, spaced at	Two CFRP plies with thickness 0.167

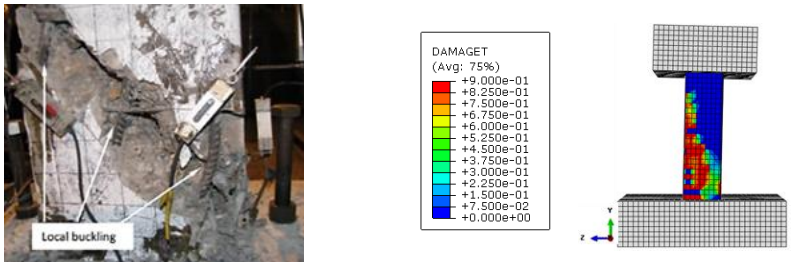

(a) Experimental result [20] (b) Finite element result

Figure 5 Comparison of control column (C0) failure in the finite element against experimental

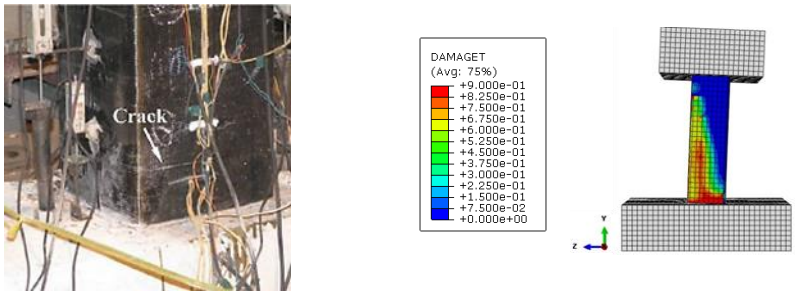

(a) Experimental result [20] (b) Finite element result

Figure 6 Comparison of CFRP-confined column (C-C2) failure in the finite element against experimental

2.5 Parametric study groups

According to the previous verification for results, it is confirmed that the proposed numerical simulation for RC rectangular columns strengthened with CFRP is reasonable. In the presented study, the numerical evaluation was executed via three groups of the tested specimens named G1, G2, and G3, where the details of specimens in group G1 only are illustrated in **Table 5**. Specimens in the group G1 are simulated the square columns, while the specimens in groups G2 and G3 are simulated the rectangular columns with a

cross-section aspect ratio 1.5 and 2 loaded in the weak direction, respectively. Also, the specimens in group G2 have a cross-section dimension of 245X367 mm, with a clear height of 817 mm and specimens in group G3 have a cross-section dimension of 212X424 mm, with a clear height of 707 mm. The chosen parameters to be studied in each group were longitudinal steel reinforcement ratio (μ_s), CFRP confinement ratio (μ_{frp}), and axial load/capacity ratio (P/P_u). Also, the axial load capacity (P_u) can be given by the following equation:

$$P_u = 0.85 f_c' (A_c - A_{sl}) + f_{sy} A_{sl} \quad (4)$$

Where, A_c and A_{sl}, f_c', and f_{sy} are the gross cross-sectional area of the column, the total area of longitudinal steel reinforcement, the unconfined compressive concrete strength, and the yield strength of longitudinal reinforcement, respectively. A special nomenclature for specimens in all groups was assigned the form of (Gi-Si), in which the first character (Gi) refers to the group name, and the second character (Si) refers to the specimen name. Furthermore, the dimensions and reinforcement details of the tested specimens were illustrated in **Figure 8**.

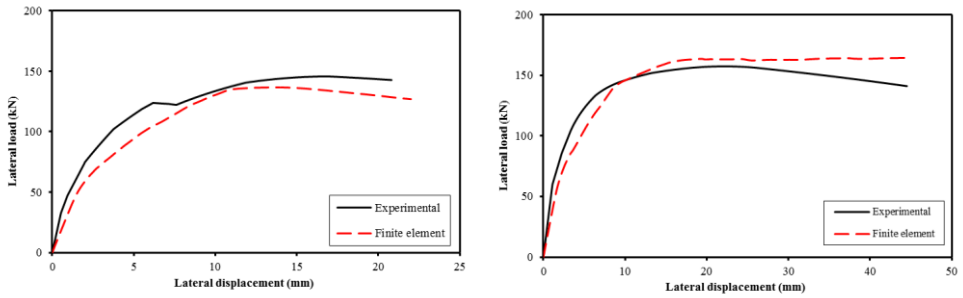

(a) Specimen (C0) (b) Specimen (C-C2)

Figure 7 Comparison of lateral load-displacement relationships in the finite element against experimental

Table 5 Description of parametric study specimens in group (G1)

Specimen code	Dimensions (bxtxh) (mm)	Longitudinal Steel			CFRP Jacket			Axial load/capacity ratio (P/Pu) %
		No. of bars	Diameter (mm)	μ_s %	t_{frp} (mm)	No. of plies	μ_{frp} %	
G1-S1	300X300X1000	8	18	2.26	0	0	0	20
G1-S2		8	18	2.26	0.167	2	0.45	20
G1-S3		8	16	1.79	0.167	2	0.45	20
G1-S4		8	20	2.79	0.167	2	0.45	20
G1-S5		8	18	2.26	0.167	3	0.67	20
G1-S6		8	18	2.26	0.167	4	0.89	20
G1-S7		8	18	2.26	0.167	2	0.45	40
G1-S8		8	18	2.26	0.167	2	0.45	60

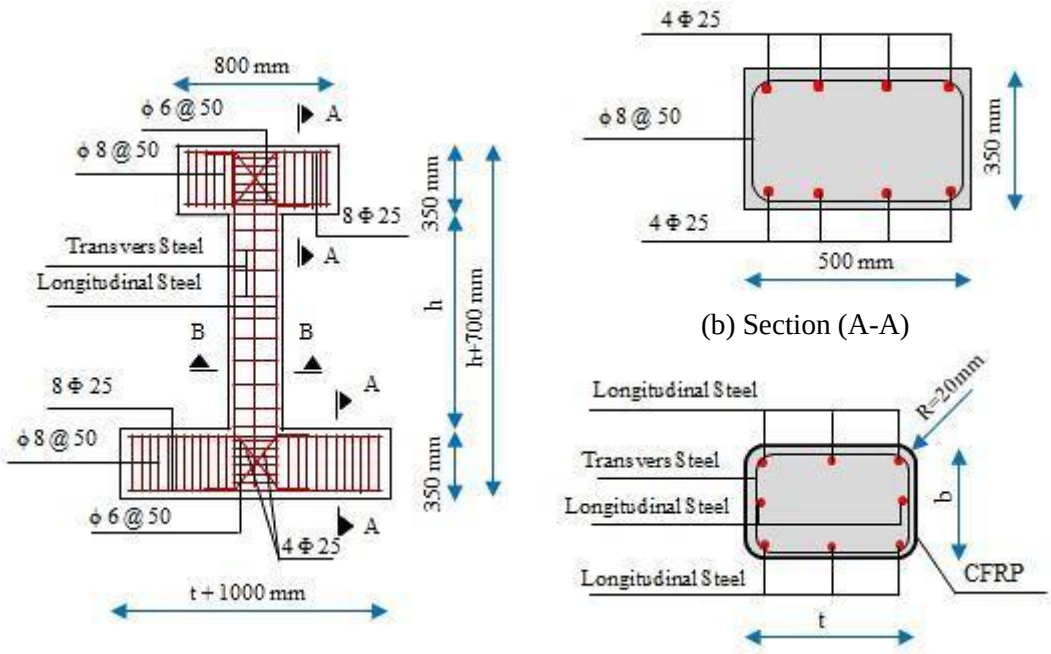

(a) Elevation view

(b) Section (A-A)

(c) Section (B-B)

Figure 8 Reinforcement details of tested specimens in the parametric study

3. Results and Discussions

3.1. Failure mode

Figure 9 shows the damage patterns of the tested specimens, in the group G1 only. For the control specimen (G1-S1), which has not any FRP confinement,

it was characterized by diagonal wide cracks, as shown in **Figure 9-a**, which is known as a shear brittle failure mode. On the other hand, for CFRP-strengthened specimens, the failure occurred at CFRP wraps rupture, which is most of the visible damage was concentrated in the critical region of the specimen and located at the bottom of the column, as shown in **Figure 9 (b-h)**. This leads to plastic hinge zone formation, which proves that FRP confinement can change the brittle shear failure mode to a flexural one for the studied cross-sections aspect ratios.

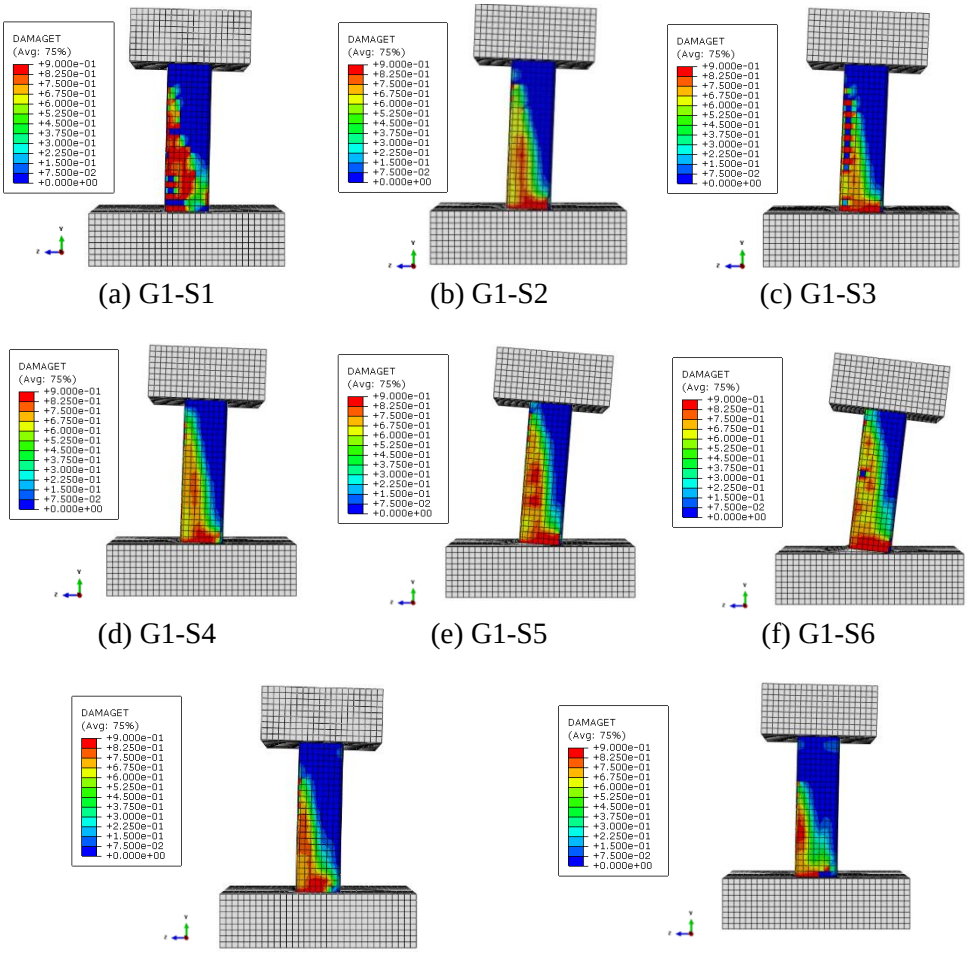

(a) G1-S1 (b) G1-S2 (c) G1-S3

(d) G1-S4 (e) G1-S5 (f) G1-S6

(g) G1-S7 (h) G1-S8

Figure 9 Cracks pattern of specimens in the group (G1)

3.2. Effect of longitudinal reinforcement ratio (μ_s)

The effect of the longitudinal reinforcement ratio (μ_s) is studied by comparing specimens Gi-S2 (μ_s=2.26%) with Gi-S3 (μ_s=1.79%), and Gi-S4 (μ_s=2.79%) in each group, as illustrated in **Table 5**. The lateral load-displacement and drift ratio relationships are presented in **Figure 10-a**, **Figure 10-b**, and **Figure 10-c** for groups G1, G2, and G3, respectively. According to the increase of the longitudinal reinforcement ratio from 1.79% to 2.26%, the lateral load capacity increases by 11.9%, 11.1%, and 13.4% for groups G1, G2, and G3, respectively. Furthermore, with an increase in the longitudinal reinforcement ratio from 1.79% to 2.79%, the lateral load capacity increases by 26.1%, 24.1%, and 25.1% for groups G1, G2, and G3, respectively. According to these results, with an increase of the longitudinal reinforcement ratio from 1.79% to 2.26%, the ultimate lateral displacement and the ultimate drift ratio decrease by 3.8%, 5.9%, and 5.3% for groups G1, G2, and G3, respectively. Also, with the increase of longitudinal reinforcement ratio from 1.79% to 2.79%, the ultimate lateral displacement and the ultimate drift ratio decrease by 13.9%, 11.97%, and 10.2% for groups G1, G2, and G3, respectively.

3.3. Effect of CFRP confinement ratio (μ_{frp})

The CFRP confinement ratio effect (μ_{frp}) is examined by comparing specimen Gi-S1, which has no FRP confinement with specimens Gi-S2, Gi-S5, and Gi-S6, which have CFRP confinement ratios of 0.45%, 0.67%, and 0.89% respectively. **Figure 11-a**, **Figure 11-b,** and **Figure 11-c** illustrate the lateral load-displacement and drift ratio relationships for groups G1, G2, and G3, respectively. According to these figures, the lateral load capacity and the ultimate drift ratio are significantly enhanced with the increase of the CFRP confinement ratio. In other words, with an increase in the CFRP confinement ratio from zero to 0.45%, the ultimate lateral displacement increases by 102%, 71%, and 200% for groups G1, G2, and G3, respectively. Also, with an increase in the CFRP confinement ratio from 0.45% to 0.67%, the ultimate lateral displacement increases by 102%, 84%, and 75% for groups G1, G2, and G3, respectively. Moreover, with an increase in the CFRP confinement ratio from 0.45% to 0.89%, the ultimate lateral displacement increases by 162%, 156%, and 205% for groups G1, G2, and G3, respectively.

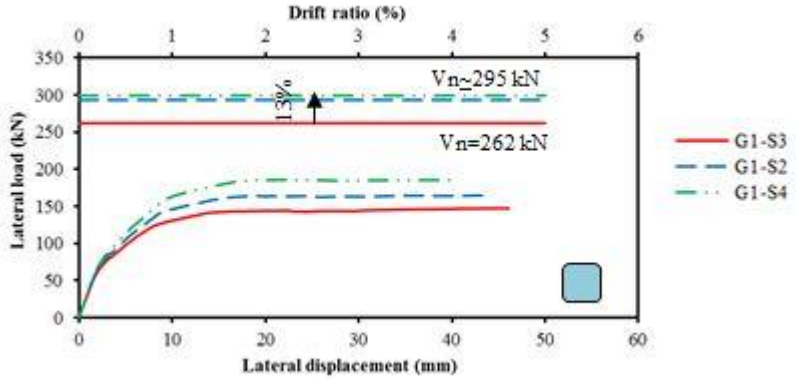

(a) Group G1

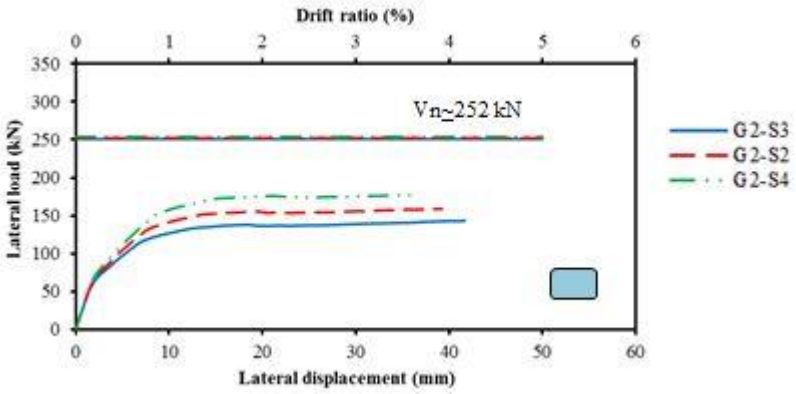

(b) Group G2

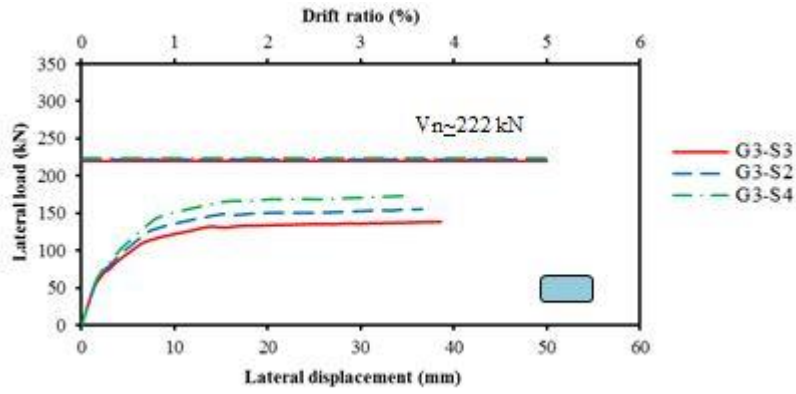

(c) Group G3

Figure 10 Effect of longitudinal reinforcement ratio on lateral load-displacement behavior

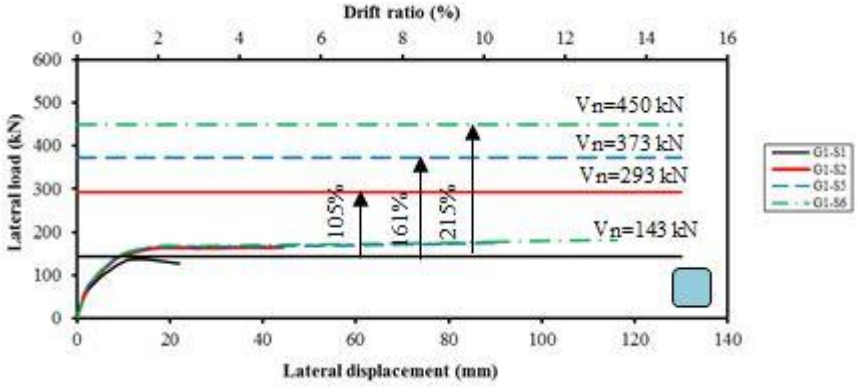

(a) Group G1

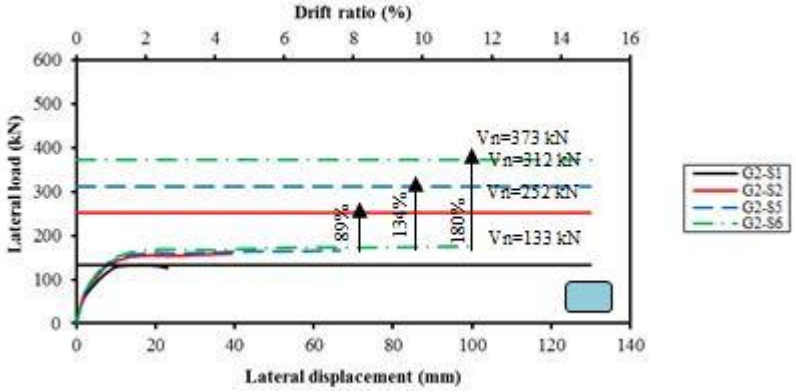

(b) Group G2

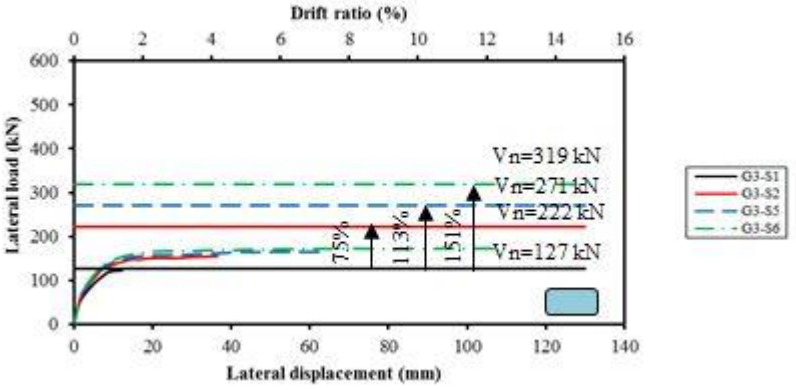

(c) Group G3

Figure 11 Effect of CFRP confinement ratio on lateral load-displacement behavior

3.4. Effect of axial load/capacity ratio (P/Pu)

The effect of the axial load/capacity ratio (P/P_u) is studied by comparing specimens Gi-S2 with axial load/capacity ratio 20% with Gi-S7 and Gi-S8, which have an axial load/capacity ratios 40% and 60%, respectively in each group. **Figure 12-a, Figure 12-b**, and **Figure 12-c** present the lateral load-displacement and drift ratio relationships for groups G1, G2, and G3, respectively. According to these results, with an increase in the axial load/capacity ratio from 20% to 40%, the lateral load capacity increases by 30%, 31%, and 31% for groups G1, G2, and G3, respectively. Also, with an increase in the axial load/capacity ratio from 20% to 60%, the lateral load capacity increases by 41%, 42%, and 39% for groups G1, G2, and G3, respectively. On the other hand, with an increase in the axial load/capacity ratio from 20% to 40%, the ultimate lateral displacement decreases by 40%, 37%, and 35% for groups G1, G2, and G3, respectively. Also, with an increase in the axial load/capacity ratio from 20% to 60%, the ultimate lateral displacement decreases by 50%, 48%, and 50% for groups G1, G2, and G3, respectively.

3.5. Evaluation of shear and flexural strengths

To evaluate the shear and flexural strengths, the nominal shear and flexural strengths (V_n and M_n) were calculated for the tested columns, according to **ACI** design codes [33, 34]. Also, the values of nominal shear strengths (V_n) are plotted in **Figure 10**, **Figure 11**, and **Figure 12** to illustrate the efficiency of CFRP-strengthening on the studied cross-section aspect ratios. It's clear from these figures that the confinement of the RC rectangular columns with CFRP sheets can be significantly enhanced their shear strength for cross-section aspect ratios 1, 1.5, and 2. **Figure 13** shows the effect of the CFRP confinement ratio of the normalized shear strength ratio (V_{max}/V_n), where, with an increase in the CFRP confinement ratio from zero to 0.45%, the normalized shear strength ratio decreases by 71%, 57%, and 39% for groups G1, G2, and G3, respectively. From the presented results, with an increase in the CFRP confinement ratio from 0.45% to 0.67%, the normalized shear strength ratio decreases by 19%, 18%, and 15% for groups G1, G2, and G3, respectively. Then, with an increase in the CFRP confinement ratio from 0.45% to 0.89%, the normalized shear strength ratio decreases by 65%, 34%, and 30% for groups G1, G2, and G3, respectively.

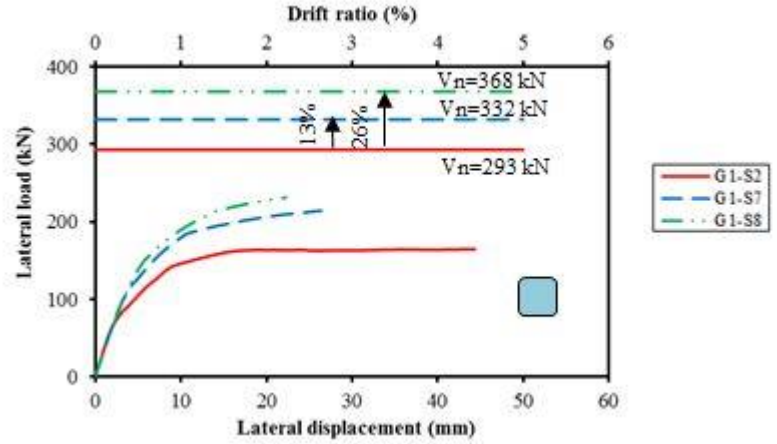

(a) Group G1

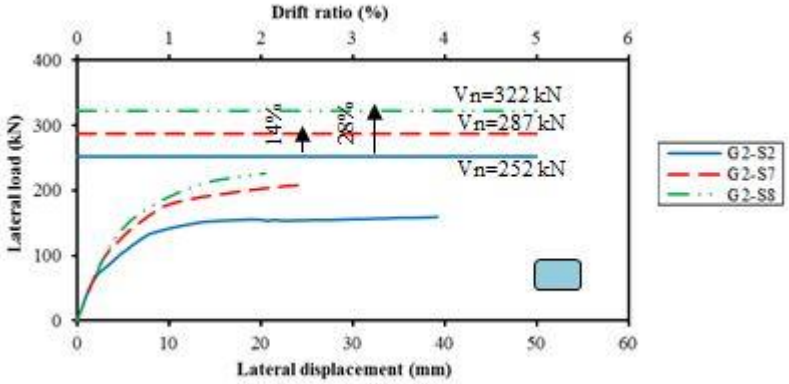

(b) Group G2

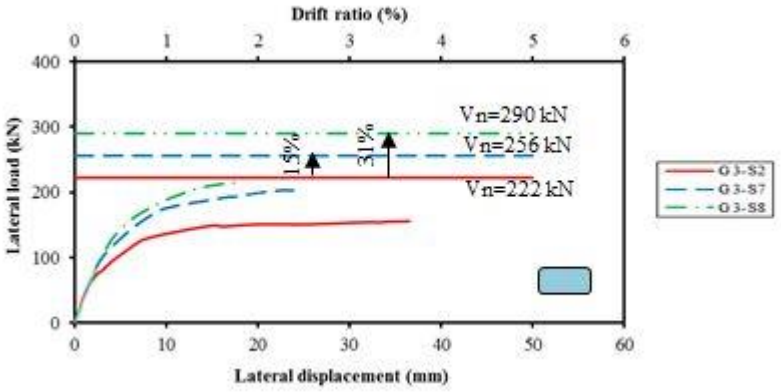

(c) Group G3

Figure 12 Effect of axial load/capacity ratio on lateral load-displacement behavior

Moreover, the effect of the CFRP confinement ratio on the normalized flexural strength ratio (M_{max}/M_n) is shown in **Figure 14**. From this figure, it is obvious that with an increase in the CFRP confinement ratio from zero to 0.45%, the normalized flexural strength ratio increases by 20%, 3%, and 5% for groups G1, G2, and G3, respectively. Furthermore, with an increase in the CFRP confinement ratio from 0.45% to 0.67%, the normalized flexural strength ratio increased by 9%, 5%, and 4.5% for groups G1, G2, and G3, respectively. Plus, with an increase in the CFRP confinement ratio from 0.45% to 0.89%, the normalized flexural strength ratio increases by 11%, 9%, and 14% for groups G1, G2, and G3, respectively.

Figure 15 presents the effect of axial load/capacity ratio on the normalized shear strength ratios for the tested columns, it's clear that with an increase in the axial load/capacity ratio from 20% to 40%, the normalized shear strength ratio increases by 16%, 15%, and 13% for groups G1, G2, and G3, respectively. On the other hand, with an increase in the axial load/capacity ratio from 40% to 60%, the normalized shear strength ratio decreases by 3%, 4%, and 7% for groups G1, G2, and G3, respectively. The effect of axial load/capacity ratio on the normalized flexural strength ratios is presented in **Figure 16**, it's observed that with an increase in the axial load/capacity ratio from 20% to 40%, the normalized flexural strength ratio increased by 29%, 31%, and 30% for groups G1, G2, and G3, respectively. Besides, with an increase in the axial load/capacity ratio from 40% to 60%, the normalized flexural strength ratio increased by 10%, 11%, and 8% for groups G1, G2, and G3, respectively.

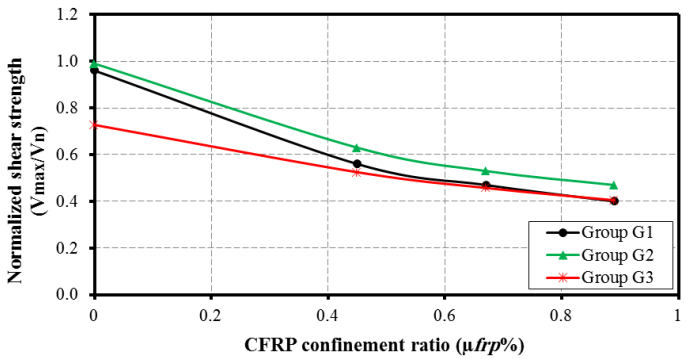

Figure 13 Effect of CFRP confinement ratio on normalized shear strength ratios

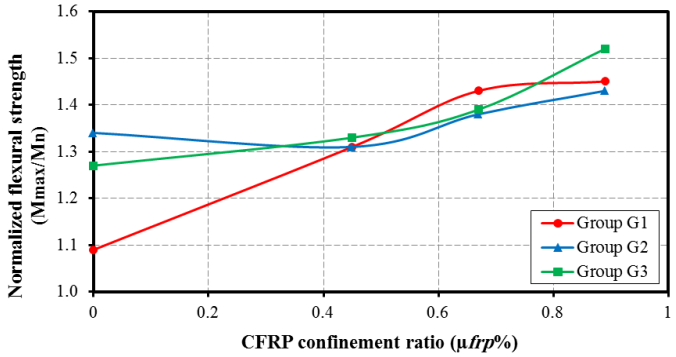

Figure 14 Effect of CFRP confinement ratio on normalized flexural strength ratios

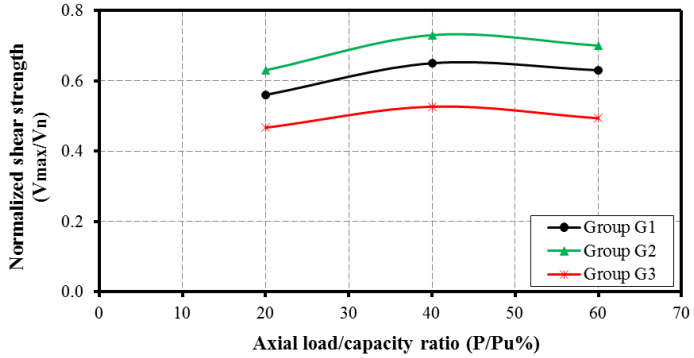

Figure 15 Effect of axial load/capacity ratio on normalized shear strength ratios

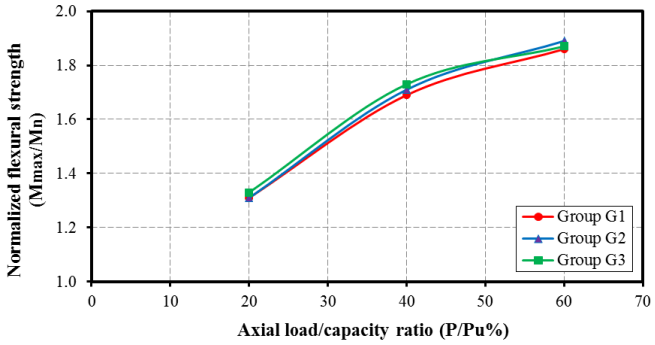

Figure 16 Effect of axial load/capacity ratio on normalized flexural strength ratios

3.6. Evaluation of drift ratio and ductility

Drift ratio is defined as the ratio of lateral displacement divided by specimen height, it's clear that with the increase of the longitudinal reinforcement ratio, the drift capacity is significantly decreased for square and rectangular

columns, as shown in **Figure 10**. In addition, with the increase of axial load/capacity ratio, the drift capacity is significantly decreased, as indicated in **Figure 12.** On the other hand, the effect of CFRP confinement is promising for increasing the drift capacity for square and rectangular columns in groups G1, G2, and G3, as shown in **Figure 11.** Regarding the ductility, it is considered a main desirable characteristic for seismic action resistance, which is the ductility can be evaluated using the displacement ductility index (μ_{Δ}), as the following equation:

$$\mu_{\Delta} = \Delta_u/\Delta_y \quad (5)$$

Where, Δ_u and Δ_y are the ultimate and yield lateral displacement, respectively. **Figure 17** shows the effect of the longitudinal reinforcement ratio on the ductility. Accordingly, with an increase in the longitudinal reinforcement ratio from 1.79% to 2.26%, the ductility index decreases by 12%, 1 %, and 14% for groups G1, G2, and G3, respectively. Also, with an increase in the longitudinal reinforcement ratio from 1.79% to 2.79%, the ductility index decreases by 26%, 16%, and 13% for groups G1, G2, and G3, respectively.

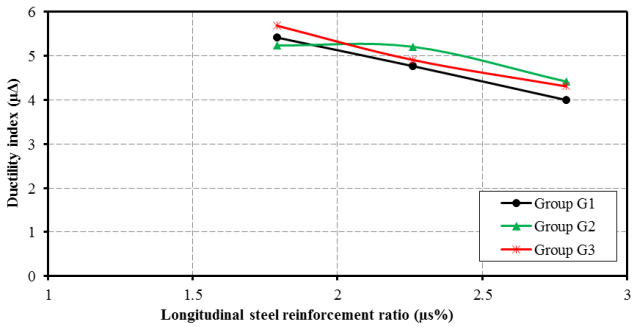

Figure 17 Effect of longitudinal reinforcement ratio on ductility index values

Moreover, **Figure 18** shows the effect of the CFRP confinement ratio on ductility, consequently, with an increase in the CFRP confinement ratio, the ductility index is significantly enhanced. In other words, with an increase in the CFRP confinement ratio from zero to 0.45%, the ductility index increases by 113%, 154%, and 236% for groups G1, G2, and G3, respectively. Also, with an increase in the CFRP confinement ratio from 0.45% to 0.67%, the ductility index increases by 108%, 63%, and 79% for groups G1, G2, and G3, respectively. Also, with an increase in the CFRP confinement ratio from

0.45% to 0.89%, the ductility index increases by 173%, 112%, and 225% for groups G1, G2, and G3, respectively.
On the other hand, the ductility index has an inverse relationship with the axial load/capacity ratio, as shown in **Figure 19**. In other words, with an increase in the axial load/capacity ratio from 20% to 40%, the ductility index decreases by 47%, 50%, and 47% for groups G1, G2, and G3, respectively. Also, with an increase in the axial load/capacity ratio from 20% to 60%, the ductility index decreases by 48%, 56%, and 71% for groups G1, G2, and G3, respectively.

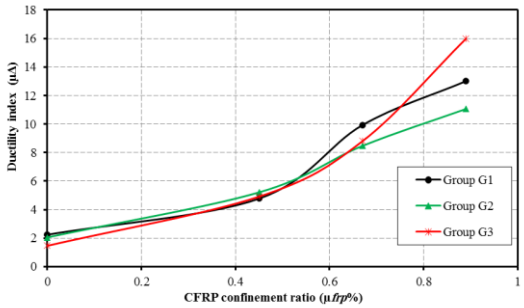

Figure 18 Effect of CFRP confinement ratio on ductility index values

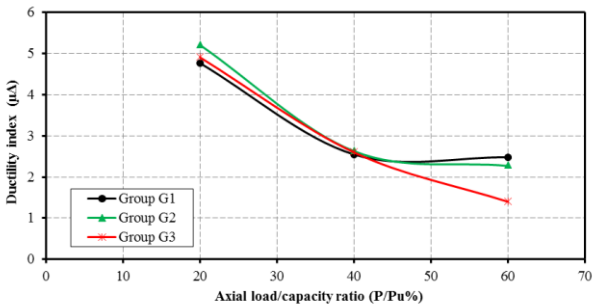

Figure 19 Effect of axial load/capacity ratio on ductility index values

4. Conclusions

The seismic performance of RC rectangular columns strengthened with CFRP wrapping was studied in this research. Based on the obtained numerical analysis results, the following conclusions can be drawn:

1. Increasing cross-section aspect ratios of the strengthened RC rectangular columns from 1 to 1.5, and 2, does not influence the shifting of their shear failure mode to a flexural one for the same number of CFRP confinement layers.

2. Confinement with CFRP wraps significantly enhances the nominal shear strength for the studied columns, but the increasing ratios in shear strength have an inverse relationship with the increase of cross-sections aspect ratios from 1 to 1.5, and 2, due to decreasing of column cross-section depth.
3. The strengthening of RC rectangular columns with CFRP jacket improves the flexural strength of the studied groups, even though it decreases with increasing the column cross-section aspect ratio, because of reducing column cross-section flexural stiffness in the lateral load direction.
4. Study results proved that the increase in the axial load/capacity ratio significantly decreases the drift capacity ratios for all studied columns cross-section aspect ratios, however, it increased with the increasing of the column cross-section aspect ratios from 1 to 1.5, and 2, under lateral load in the weak direction of column cross-section.

References

[1] Kocak, A., The effect of short columns on the performance of existing buildings. Structural Engineering and Mechanics, 2013. 46(4): pp. 505-518.
[2] Guevara, L.T. and L.E. Garcı´a, The Captive- and Short-Column Effects. Earthquake Spectra, 2005. 21(1): pp. 141-160.
[3] Biskinis, D.E., G.K. Roupakias, and M.N. Fardis, Degradation of shear strength of reinforced concrete members with inelastic cyclic displacements. Structural Journal, 2004. 101(6): pp. 773-783.
[4] Vandoros, K.G. and S.E. Dritsos, Concrete jacket construction detail effectiveness when strengthening RC columns. Construction and Building Materials, 2008. 22(3): pp. 264-276.
[5] Ma, C.-K., et al., Repair and rehabilitation of concrete structures using confinement: A review. Construction and Building Materials, 2017. 133: pp. 502-515.
[6] Islam, N., and M. Hoque, Strengthening of Reinforced Concrete Columns by Steel Jacketing: A State of Review. Asian Transactions on Engineering (ATE ISSN: 2221-4267) Volume, 2015. 5.
[7] Belal, M.F., H.M. Mohamed, and S.A. Morad, Behavior of reinforced concrete columns strengthened by steel jacket. HBRC Journal, 2015. 11(2): pp. 201-212.
[8] Nanni, A. and J. Giancaspro, FRP composites for reinforced and prestressed concrete structures: a guide to fundamentals and design for repair and retrofit. 2009: Taylor & Francis.
[9] Harajli, M. and F. Dagher, Seismic strengthening of bond-critical regions in rectangular reinforced concrete columns using fiber-reinforced polymer wraps. Aci Structural Journal, 2008. 105: pp. 68-77.

[10] Gora, A.u.M., et al., Finite element analysis of rectangular reinforced concrete columns wrapped with FRP composites. IOP Conference Series: Materials Science and Engineering, 2018. 431: pp. 072005.
[11] Wu, Y.-F. and Y.-Y. Wei, Effect of cross-sectional aspect ratio on the strength of CFRP-confined rectangular concrete columns. Engineering Structures, 2010. 32(1): pp. 32-45.
[12] Farrokh Ghatte, H., et al., Seismic Retrofit of Full-Scale Substandard Extended Rectangular RC Columns through CFRP Jacketing: Test Results and Design Recommendations. Journal of Composites for Construction, 2018. 23(1): pp. 04018071.
[13] Del Zoppo, M., et al., FRP for seismic strengthening of shear-controlled RC columns: Experience from earthquakes and experimental analysis. Composites Part B: Engineering, 2017. 129: pp. 47-57.
[14] Oucif, C., et al., Numerical modeling of reinforced concrete strengthened columns under cyclic loading. Arabian Journal for Science and Engineering, 2017. 42(9): pp. 3933-3944.
[15] Juntanalikit, P., T. Jirawattanasomkul, and A. Pimanmas, Experimental and numerical study of strengthening non-ductile RC columns with and without lap splice by Carbon Fiber Reinforced Polymer (CFRP) jacketing. Engineering Structures, 2016. 125: pp. 400-418.
[16] Realfonzo, R. and A. Napoli, Results from cyclic tests on high aspect ratio RC columns strengthened with FRP systems. Construction and Building Materials, 2012. 37: pp. 606-620.
[17] Ozcan, O., B. Binici, and G. Ozcebe, Seismic strengthening of rectangular reinforced concrete columns using fiber reinforced polymers. Engineering Structures, 2010. 32(4): pp. 964-973.
[18] ElGawady, M., et al., Retrofitting of rectangular columns with deficient lap splices. Journal of Composites for Construction, 2009. 14(1): pp. 22-35.
[19] Galal, K., A. Arafa, and A. Ghobarah, Retrofit of RC square short columns. Engineering Structures, 2005. 27(5): pp. 801-813.
[20] Ouyang, L.-J., et al., Seismic retrofit of square reinforced concrete columns using basalt and carbon fiber-reinforced polymer sheets: A comparative study. Composite Structures, 2017. 162: pp. 294-307.
[21] ABAQUS, Analysis User's Manual, in Dassault SystÈmes Simulia Corp., Providence, RI, V. 6.12-1, Editor. 2012.
[22] Papanikolaou, V.K. and A.J. Kappos, Confinement-sensitive plasticity constitutive model for concrete in triaxial compression. International Journal of Solids and Structures, 2007. 44(21): pp. 7021-7048.
[23] Hany, N.F., E.G. Hantouche, and M.H. Harajli, Finite element modeling of FRP-confined concrete using modified concrete damaged plasticity. Engineering Structures, 2016. 125: pp. 1-14.
[24] Tao, Z., Z.-B. Wang, and Q. Yu, Finite element modelling of concrete-filled steel stub columns under axial compression. Journal of Constructional Steel Research, 2013. 89: pp. 121-131.

[25] Yuan, F., Y.-F. Wu, and C.-Q. Li, Modelling plastic hinge of FRP-confined RC columns. Engineering Structures, 2017. 131: pp. 651-668.
[26] Ozbakkaloglu, T., A. Gholampour, and J.C. Lim, Damage-Plasticity Model for FRP-Confined Normal-Strength and High-Strength Concrete. Journal of Composites for Construction, 2016. 20(6): pp. 04016053.
[27] Saenz, L.P., discussion of" Equation for the Stress-Strain Curve of Concrete" by Desayi and Krishnan. Journal of the American Concrete Institute, 1964. 61: pp. 1229-1235.
[28] Ferrotto, M., O. Fischer, and L. Cavaleri, A strategy for the finite element modeling of FRP-confined concrete columns subjected to preload. Engineering Structures, 2018. 173: pp. 1054-1067.
[29] Popovics, S., A numerical approach to the complete stress-strain curve of concrete. Cement and Concrete Research, 1973. 3(5): pp. 583-599.
[30] Wahalathantri, B.L., et al. A material model for flexural crack simulation in reinforced concrete elements using ABAQUS. in Proceedings of the first international conference on engineering, designing, and developing the built environment for sustainable wellbeing. 2011. Queensland University of Technology.
[31] Taghia, P. and S.A. Bakar, Mechanical behaviour of confined reinforced concrete-CFRP short column-based on finite element analysis. World Applied Sciences Journal, 2013. 24(7): pp. 960-970.
[32] [32] Hajsadeghi, M., F.J. Alaee, and A. Shahmohammadi, Investigation on Behaviour of Square/Rectangular Reinforced Concrete Columns Retrofitted with FRP Jacket. Journal of Civil Engineering and Management, 2011. 17(3): pp. 400-408.
[33] Institute, A.C., Building code requirements for structural concrete (ACI 318-11) and commentary. ACI 318R-11, Farmington Hills, MI, 2011.
[34] Guide for the Design and Construction of Externally Bonded FRP Systems for Strengthening Concrete Structures: ACI 440.2 R-02. 2002. American Concrete Institute.

دراسة نظرية لتقييم الأداء الزلزالي للأعمدة الخرسانية المسلحة المستطيلة و المقواة بقمصان البوليمرات المسلحة بألياف الكربون

الملخص العربي:

إن الهدف الرئيسي من هذه الدراسة هو معرفة وتقييم الأداء الزلزالي للأعمدة الخرسانية المستطيلة المدعمة بقمصان البوليمرات المسلحة بألياف الكربون (CFRP) تحت تأثير حمل رأسي ثابت وحمل عرضي يزيد تدريجيا حتى الانهيار. إن هذا التقييم يهدف إلى فحص ودراسة تأثير بعض المتغيرات مثل نسبة التسليح الرأسي، نسبة حجم تسليح البوليمرات المسلحة بألياف الكربون، نسبة الحمل الرأسي المؤثر/ مقاومة العمود على السلوك الزلزالي للأعمدة الخرسانية المسلحة المستطيلة المقواة بقمصان البوليمرات المسلحة بألياف الكربون. تم تشييد نماذج التحليل العددي ثلاثي الأبعاد باستخدام نظرية العناصر المحددة باستخدام برنامج (ABAQUS) لتمثيل الأعمدة الخرسانية المسلحة المستطيلة المقواة بقمصان البوليمرات المسلحة بألياف الكربون، وتم مقارنه نتائج التحليل العددي مع الأبحاث المعملية وأظهرت المقارنة توافقا" مع النتائج المعملية. من خلال تحليل النتائج يمكن القول بانه كلما زادت نسبة التسليح الرأسي تزيد قدرة التحميل العرضي للأعمدة، بينما تقل قيم أقصي إزاحة جانبية والممطولية بشكل ملحوظ. بالإضافة لذلك، أثبتت النتائج أنه بزيادة نسبة حجم تسليح البوليمرات المسلحة بألياف الكربون تزيد قدرة التحميل العرضي، أقصي ازاحة جانبية، الحركة النسبية للعمود، الممطولية مما يعزز السلوك الزلزالي للأعمدة المقواة بألياف البوليمرات المسلحة بالكربون بشكل كبير. أظهرت نتائج الدراسة أن زيادة نسبه الحمل الرأسي المؤثر/ مقاومة العمود تزيد من قدرة التحميل العرضي، بينما تقلل بشكل كبير من قيم الحركة النسبية للعمود والممطولية.